

SUSTAINABLE ADSORPTIVE REMOVAL OF NICKEL AND CHROMIUM USING AN ECO-FRIENDLY INDUSTRIAL WASTE: A KINETIC STUDY

Yehia H. Magdy¹, Hossam Altaher², Anwar F. Al Yaqout³

¹ Department of Chemical Engineering, Faculty of Engineering,
El-Minia University P.O. Box 61511, Egypt

Received 28 November 2018

² Sustainable Solution Group, Al-Sharq, Ahmed Al-Jaber St., Al-Dira Tower,
P.O.Box 17886 – Khalidiyah Code: 72459, Kuwait
E-mail: haltaher1970@gmail.com

Accepted 31 January 2019

³ Civil Engineering Department, Kuwait University
P.O. Box 5969 Safat – 13060 Kuwait,
E-mail: aalyaqout@yahoo.com

ABSTRACT

Due to the high cost of activated carbon as an adsorbent, there is a growing interest in a search of alternative sustainable adsorbents. The objective of this study is to investigate the potential use of fuller's earth (a solid waste from vegetable oils industry) as an adsorbent for chromium and nickel ions.

The adsorption is investigated under different experimental conditions referring to the initial concentration (2 - 12 mg/L), the adsorbent dose (0.15 - 1.8 g/L), and the contact time (0 - 360 min). The adsorption kinetics is examined using the pseudo first order, the pseudo second order, the Elovich, the intraparticle diffusion, and the Boyd models. The equilibrium is attained within 240 min. The adsorption of chromium and nickel ions is found to have a chemical nature as revealed by the Elovich and the pseudo second order models. The results obtained show that the adsorption mechanism of chromium ions refers predominantly to intraparticle diffusion, while both intraparticle diffusion and film diffusion are found to control the adsorption of nickel ions.

Keywords: adsorption, Fuller's earth, industrial wastes, kinetic models, sustainability, wastewater.

INTRODUCTION

Wastewater from industrial facilities around the world contains high levels of toxic heavy metals such as chromium, lead, mercury, cadmium, nickel, and cobalt. This wastewater is usually disposed as surface water. If this wastewater is not well treated prior to the disposal, it can cause a detrimental impact on the ecosystem and consequently on public health.

Hexavalent chromium which is the toxic form of chromium may be found in the effluents of various industries including fertilizers production, electroplating, leather tanning, mining, cement, dyeing, and photography [1]. The concentration of hexavalent chromium

in these effluents may cause severe environmental and public health problems. This toxic form of chromium may cause acute and chronic adverse effects in warm-blooded animals [1]. The adverse effects include toxic, allergenic, irritant, and carcinogenic one and are harmful by all exposure routes [2, 3]. Moreover, chromium has an indirect adverse effect due to its bioaccumulation behavior, environmental persistence, and carcinogenicity [4]. USEPA and the European Union recommend a tolerance limit of surface wastewater of below 0.05 mg/l [1].

Even though nickel is an essential element in human bodies and for plants growth [5], the excessive nickel concentration in the organism is very toxic. Its adverse effects include dermatitis, myocarditis, encephalopathy,

pulmonary fibrosis, headache, dizziness, nausea and vomiting, chest pain, rapid respiration, and lungs cancer [6, 7].

Many anthropogenic activities such as metal processing, mining, land-application of sewage sludge are potential sources of wastewater containing this metal [8, 9].

The heavy metals removal from the wastewater can be done using physical, chemical, or biological techniques. Examples of the treatment techniques refer to a chemical precipitation, a coagulation, a membrane filtration, an electrochemical treatment, an ion exchange, an oxidation by biological means, a catalytic degradation, and an adsorption [10, 11].

Among those, the adsorption is considered the most effective methodology. Its advantages include the low cost, the flexibility, the simplicity of the design, and the ease of operation [12, 13]. In addition, the adsorption has an effective removal efficiency in respect to different pollutants even at low concentrations [14]. Activated carbon is the most widely used adsorbent. However, it has many drawbacks like high production and regeneration costs [15, 16]. The critical point in selecting an alternative adsorbent is to find a low-cost material that is readily available in large quantities and has a high removal efficiency in respect to the pollutant investigated [17, 18].

Fuller's earth is natural clay that is used in the vegetable oil industry as a bleaching agent. It has a single use in this industry. After the bleaching stage of the vegetable oils, the spent fuller's earth is separated by filtration and thrown to dumps [19].

Using solid waste materials as an adsorbent for treating wastewater is an economic alternative of the activated carbon. The goal of the present research is to evaluate the removal efficiency of fuller's earth as an industrial solid waste in respect to chromium and nickel present in the wastewater. Furthermore, the different factors affecting the adsorption are studied. Different kinetic models are investigated to determine the rate and mechanism of adsorption.

EXPERIMENTAL

Adsorbent

Fuller's earth was obtained from Oil and Fats Manufacturing Factory in Cairo, Egypt. This material was used in the oil industry as a bleaching material to remove dyes. After the bleaching process, the fuller's

earth was separated by filtration and discarded as a solid cake. The samples received from the factory were covered by oil and fats. To remove these impurities they were subjected to prolonged washing with ethanol and air-drying at a room temperature.

Adsorbate

The wastewater was prepared by dissolving chromium and nickel salts (analytical grade) in bi-distilled water. The chromium and nickel concentrations were determined prior to and after the adsorption by an atomic adsorption spectroscopy using a Scan AA4 instrument (Thermo Jarrell Ash, Franklin, MA, USA).

Batch study

A batch adsorber vessel as illustrated in Fig. 1 was used in all experiments. The vessel was filled with 1700 cm³ of the wastewater solution investigated. Batch adsorption studies were carried out for chromium and nickel removal. The factors studied referred to the adsorbent mass (0.25 g - 2 g equivalent to doses 0.15 g/L - 1.18 g/L), the initial concentration (4 mg/L - 12 mg/L), and the contact time (0 min - 360 min). A large baker containing 1700 mL of wastewater was used to perform the batch study. All experiments were conducted at a room temperature ($25 \pm 2^\circ\text{C}$). The agitation speed was

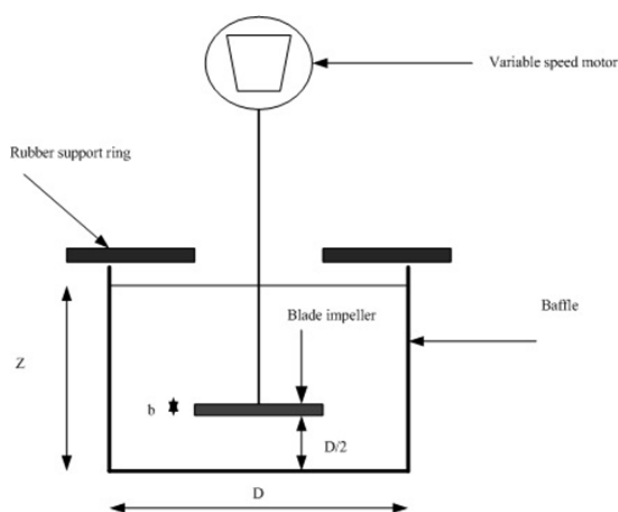


Fig. 1. Schematic diagram of the bath adsorber vessel, D = diameter of vessel (13 cm), b height of impeller blade ($0.01 D$), Z = height of liquid in vessel (20 cm).

Table 1. Equations and parameter and kinetic models.

Kinetic model	Parameters	Reference
Pseudo first order $\ln(q_e - q_t) = \ln q_e - k_1 t$	q_e, q_t (mg/g) are adsorption capacities at equilibrium and at any time t (min), respectively; and k_1 (min^{-1}) is the rate constant of the pseudo first order equation	[20]
Pseudo second order $t/q_t = 1/k_2 q_e^2 + t/q_e$ $h = k_2 q_e^2$	k_2 (g/mg.min) is the rate constant of the pseudo second order equation, q_e (mg/g) is the maximum adsorption capacity, q_t (mg/g) is the amount adsorbed at time t (min), h is regarded as the initial sorption rate when t approaches 0	[21]
Elovich $q_t = 1/B \ln(\alpha B) + 1/B \ln t$	α (mg/g min) is the initial adsorption rate and B (g/mg) is the adsorption constant related to the extent of the surface coverage and activation energy for chemisorption	[20]
Intraparticle diffusion $q_t = k_{id} t^{0.5} + C$	q_t (mg/g) is the amount adsorbed at time t (min), k_{id} ($\text{mg/g.min}^{0.5}$) is the rate constant for the intraparticle diffusion model, and C (mg/g) is a constant related to the boundary layer resistance to diffusion	[22, 23]
Boyd model $B_t = -0.4977 - \ln(1 - q_t/q_e)$	q_e, q_t (mg/g) are the amounts of dye adsorbed at equilibrium and at any time t (min), B_t is the mathematical function of fractional attainment of equilibrium	[20]

kept at 400 rpm in all tests. The samples were filtered prior to the analysis to separate the adsorbent.

To study the effect of the adsorbent dose, four quantities of the adsorbent (0.25 g, 0.5 g, 1.0 g, and 2.0 g) were used. The initial concentration of the heavy metals in each vessel was adjusted to 10 mg/L. The vessels were agitated for 4 h to reach an equilibrium. The samples were taken from the beakers and analyzed for the respective pollutant.

A similar series of batch adsorbers were used to study the effect of the initial metal concentration. The wastewater in every adsorber was adjusted at a certain metal concentration (4 mg/L - 12 mg/L) by adding a pure metal solution. A fixed mass of adsorbent was added to every adsorber. The mixtures were agitated till an equilibrium was attained as discussed above.

The effect of the agitation time was tested by the same technique. 10 mL samples were taken from the tanks at different time intervals, they were filtered and analyzed to determine the final concentration.

Mathematical models

The batch data were analyzed using 5 kinetic models. They were the pseudo first order, the pseudo second order, the Elovich, the intraparticle diffusion, and the

Boyd model. The linear equations of these models are presented in Table 1.

RESULTS AND DISCUSSION

Characterization of the adsorbent

The fuller's earth is an economical material that is commercially available, eco-friendly, and non-toxic [24]. It is a sedimentary clay that has hydrous aluminum silicate $[(\text{OH}_4)\text{Si}_8\text{O}_{20}\cdot n\text{H}_2\text{O}]$ as its main component [25]. The concentration of the hydrous aluminum silicate varies from one ore to another. The other minerals that may be present in the fuller's earth include quartz, calcite, and dolomite [26, 27]. Two types of charges contribute to the total charge of the clay minerals; the structural and the surface one. The structural charge is due to ion substitutions and it is permanent. The surface charge depends on the pH value [27]. The crystalline structure of the clay consists of three layers; two silica layers alternating with one alumina or silica one. The negative charge on the surface is due to the isomorphous substitution of Si_4 by Al_3 in the tetrahedral sheet [28].

In general, the structure consists of layers of tetrahedral silicon and octahedral aluminum or magnesium bound oxygen and hydroxyls [29]. The properties of the

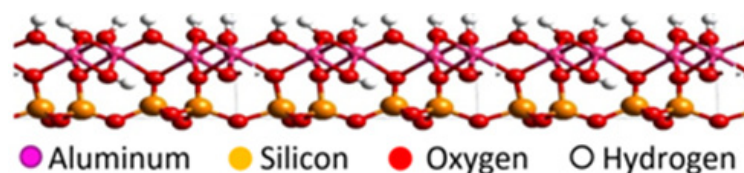


Fig. 2. Example of Molecular structure of aluminum silicate (the main constituent of fuller's earth).

Table 2. Physical properties of fuller's earth [28].

Property	Value
Surface area	120-140 m ² /g
Porosity	60-70%
Cation exchange capacity	50-200 meq/100 g
Exchangeable cations	Na ⁺ , K ⁺ , H ⁺ , Mg ²⁺ , Ca ²⁺ ,
Mean equivalent diameters of pores	190-200 Å
Particle size	10 μm

fuller's earth are given in Table 2. An example of the molecular structure of aluminum silicate is illustrated in Fig. 2.

An effect of the mixing time

The effect of the mixing time on the removal of chromium and nickel is illustrated by Fig. 3. It is clear that the adsorption uptake increases with the increase of the contact time. The equilibrium is attained within 240 min for both ions. Two adsorption stages can be identified. During the rapid initial stage the adsorption process is fast. Within 60 min 65 % of the nickel ions are removed, while 50 % of the final chromium concentration is reached within the same time interval. After this initial stage, the adsorption proceeds slowly. The initial rapid adsorption stage may be attributed to the abundance of many active sites existing on the surface of the adsorbent. Fig. 3 indicates that even though both adsorption systems have reached the equilibrium plateau within the same time (240 min), the adsorption uptake of nickel is almost two times that of chromium. The concentration gradient, which is high during the initial stage, is another reason for the rapid proceeding. This concentration gradient acts as a driving force of the adsorption and it decreases with time [30].

An effect of the initial concentration

It is clear from Fig. 4 that the increase of the initial concentration has a pronounced effect on the adsorption capacity. The increase of the chromium initial concentration from 4 mg/L to 12 mg/L results in an increase of the adsorption capacity from 3.5 mg/g to 9 mg/g (a ratio of around 3). A similar response of this increase is observed in case of nickel ions. An increase of the initial concentration from 6 mg/L to 12 mg/L results in doubling the adsorption capacity. On the other hand, the effect of the initial concentration on the equilibrium time is different for the two adsorbates. While the initial concentration does not have a significant effect in case of chromium ions adsorption, it has a considerable effect on that of nickel ions. As evident, the equilibrium time increases from 90 min when the initial concentration is 6 mg/L to 240 min when the initial concentration is increased to 12 mg/L.

The chemical driving force plays an important role in the adsorption process. The high concentration of the metal ions (consequently a high driving force) will accelerate the adsorption process due to the rapid ions diffusion through the adsorbent pores. At later stages and with the decrease of the concentration due to the adsorption process, the driving force will decrease and

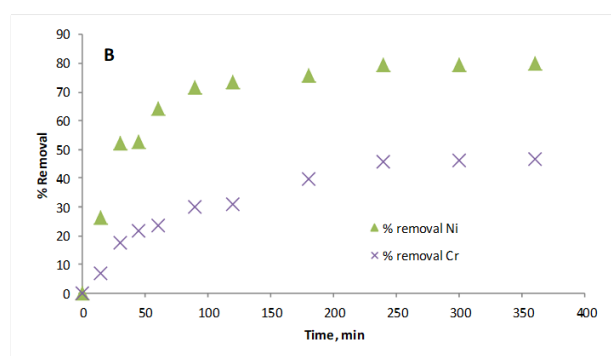
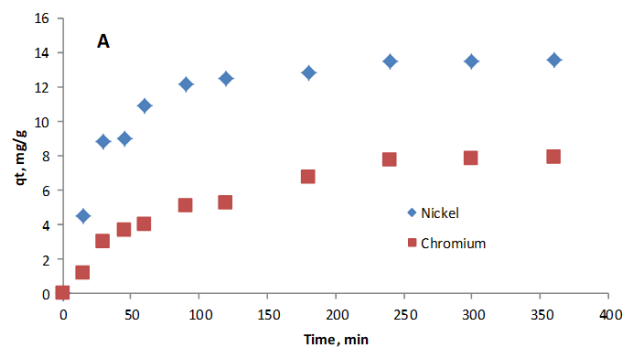


Fig. 3. Effect of mixing time on nickel and chromium adsorption.

consequently, the adsorption rate will decrease. It is clear from Fig. 4 that the initial concentration of both ions does not affect the initial uptake rate. This is due to the availability of a sufficient number of vacant adsorption sites accommodating the ions in the solution. In such a case, no competition occurs between the ions [15].

An effect of the adsorbent dose

The adsorbent dosage is a critical parameter in the adsorption process design. This parameter gives an indication of the effectiveness of the adsorbent and the ability of the adsorbate to be adsorbed in presence of a minimum dosage. It is clear from Fig. 5 that the increase of the adsorbent dose from 0.15 g/L to 1.18 g/L results in a decrease of the nickel amount adsorbed from 49.0 mg/g to 6.88 mg/g. On the other hand, the adsorption removal efficiency in respect to chromium increases from 72.05 % to 81 % with the increase of the adsorbent dose from 0.15 g/L to 1.18 g/L. It is clear that the adsorption capacity of chromium and nickel is a function of the adsorbent dose. For chromium, the increase of the dose from 0.15 g/L to 1.18 g/L results in

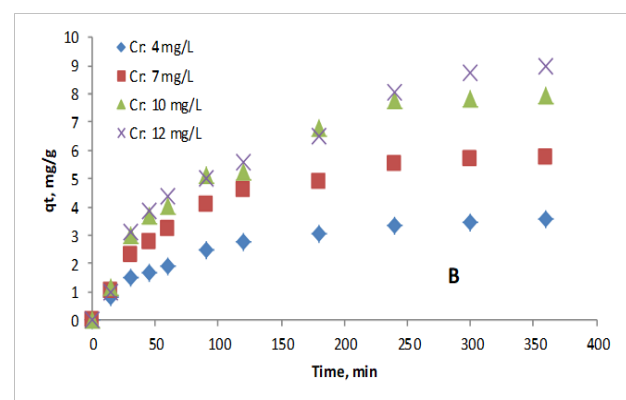
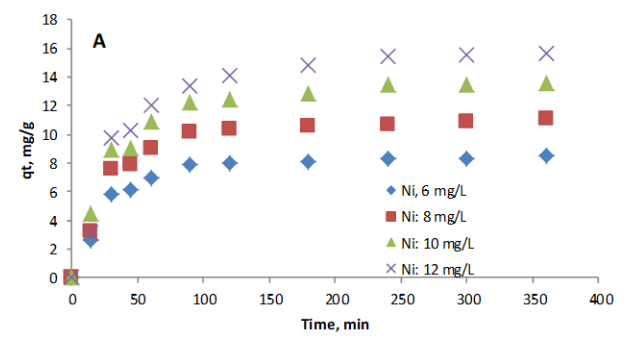


Fig. 4. Effect of initial nickel (A) and chromium (B) concentration on their adsorption.

a decrease of the adsorption capacity from 19.22 mg/g to 4.6 mg/g. An increased adsorbent quantity means more pores and consequently more available active sites. The adsorbates' ions will not have to compete on a limited number of active sites. Moreover, the presence of a large amount of an adsorbent in the solution will hinder the homogeneous distribution of the adsorbent and some of the active sites will not be available.

The small particle sizes of the adsorbent (10 μm) has a positive effect on the adsorption of nickel and chromium ions. Moreover, as illustrated in Table 2, the mean equivalent diameters of the fuller's earth pores are in the range 190 \AA - 200 \AA (mesopores). Compared to the ionic radii of nickel and dichromate ions which are 0.69 \AA and 2.92 \AA , the pore diameter of the adsorbent does not represent any restriction

As illustrated by Fig. 5, the relationship between the adsorption capacity (q) and the adsorbent dose (D) deviates from linearity. The regression coefficients (R^2) for nickel and chromium ions are found equal to 0.74 and 0.80, respectively. The linear relation between q and (D) is described by the equation ($q = sD + I$). The intercept

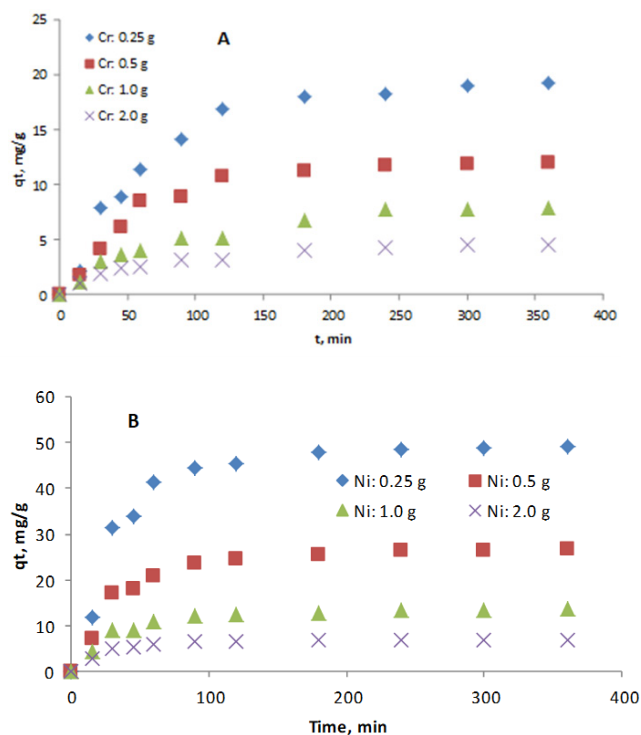


Fig. 5. Effect of time on adsorption of chromium (A,B) and nickel (C,D).

(I) represents the maximum adsorption capacity when the adsorbent dose approaches zero, while the slope (s) is related to the sorption potential of the adsorbent. The values of (s) for chromium and nickel adsorption are -12.45 and -35.21, respectively. The negative value in both cases indicates a decrease of the adsorption capacity with an increase of the adsorbent dose [12]. As illustrated by Fig. 5 (b) and Fig. 5 (d) the adsorbent dose does not have a significant effect on either the adsorption rate or the equilibrium time for both ions.

There is another important factor to be taken into consideration in the course of the adsorbent dose discussion. It refers to the large surface area and the negative surface charge of the fuller's earth. The increased adsorbent dose provides more active sites for the adsorption of the positively charged adsorbates [31].

Kinetic analysis

The kinetic analysis of the adsorption process describes the adsorbate uptake rate, the equilibrium time required for the adsorption process, and the mechanisms of the process. The identification of these factors is important in designing and scaling up the

adsorption. The rate and the mechanism of the adsorption process are investigated in the present study by fitting the experimental data to pseudo first order, pseudo second order, Elovich intraparticle diffusion, and Boyd models.

Rate equations

The comparison of the results listed in Table 3 indicates that the pseudo second order kinetic model fits the experimental data better than the pseudo first order one. This is illustrated by the high R^2 values and the conformation between the adsorption capacity ($q_{t,calc}$) calculated on the ground of the model, and the experimental adsorption capacity ($q_{t,exp}$). These results reveal that the pseudo first order model is not applicable to the adsorption kinetics of chromium and nickel ions onto fuller's earth. The observed deviation (in case of a pseudo first order model) from the experimental data may be attributed to the sharp fall of the ion concentration after the initial fast adsorption at the onset of the adsorption process due to the availability of a large number of active sites on the surface of the adsorbent [32]. Furthermore, the fitting of the data to the pseudo-second order kinetic model indicates the chemical nature of the adsorption of both ions on the adsorbent [33, 34]. Accordingly, a chemical bonding takes place between the adsorbate ions and the adsorbent active sites [35].

The structure of the fuller's earth as illustrated by Fig. 2 can be represented as an indefinitely extended sheet of hydrated aluminum silicate. The bonds within the crystal lattice structure are covalent. The arrangement of the constituents of the crystals (aluminum, silicon, oxygen, and hydrogen) gives the structure a relatively strong negative charge. This charge is the key player in the adsorption of different cations that may be present in the wastewater and consequently it is the factor responsible for the chemical nature of the adsorption process [36].

It is also worth noting that a linear relationship is observed between the initial concentration and the rate constant (k_2) of the adsorption process for both chromium and nickel ions (data is not shown). On the other hand, this linear relationship is not fulfilled in case of the initial rate constant h_2 . As seen from Table 3, the rate constant k_2 of nickel is approximately twice that of chromium at all concentrations studied. This may explain the higher adsorption capacity in respect to nickel [37].

Table 3. Kinetic parameters for adsorption of nickel and chromium.

Model	Parameter	Nickel, mg/L				Chromium, mg/L			
		6	8	10	12	4	7	10	12
Pseudo-First-Order									
	$q_{e, calc}$ (mg/g)	3.227	5.583	9.973	11.881	3.337	6.314	9.144	9.590
	$q_{e, exp}$ (mg/g)	8.5272	11.116	13.585	15.674	3.550	5.750	7.966	8.963
	K_1 (1/min)	0.0103	0.0116	0.0181	0.0161	0.0123	0.015	0.0142	0.0107
	R^2	0.8363	0.8686	0.963	0.9772	0.9861	0.9503	0.9572	0.9334
Pseudo-Second-Order									
	$q_{e, calc}$ (mg/g)	9.001	11.806	14.619	17.544	4.21	6.949	10.20	11.26
	$q_{e, exp}$ (mg/g)	8.5272	11.116	13.585	15.674	3.550	5.750	7.966	8.963
	K_2 (g/ mgmin)	0.0054	0.0038	0.0029	0.0016	0.0038	0.0021	0.0011	0.0009
	h_2 (mg/g. min)	0.4375	0.5297	0.6198	0.4925	0.0674	0.1014	0.1144	0.1141
	R^2	0.997	0.9964	0.9983	0.9879	0.9979	0.9954	0.9848	0.9785
Elovich									
	α (mg/g.min)	11.2959	11.9783	5.9580	4.3890	0.1469	0.2227	0.2534	0.2462
	β (g/ mg)	0.9435	0.7041	0.4910	0.3949	1.1161	0.6592	0.4559	0.4092
	R^2	0.8822	0.902	0.9078	0.9548	0.9901	0.9897	0.9849	0.9807
Intraparticle Diffusion									
	k_{id}	0.2829	0.3797	0.4851	0.6417	0.1917	0.3172	0.4497	0.4954
	C	3.9686	4.9771	5.8359	5.3886	0.3321	0.4813	0.3074	0.0933
	R^2	0.6545	0.6625	0.7406	0.7226	0.9501	0.9385	0.9637	0.9768

The Elovich equation is usually used for modeling the chemical adsorption processes. It is effective for systems with a heterogeneous adsorbing surface [38]. This model has been successfully applied to explain the adsorption of many species like metal ions (cobalt,

nickel, lead, cadmium, copper, and zinc), and dyes in aqueous solutions [39]. It contains the parameter β that describes the desorption state of the adsorbate on the surface of the adsorbent. The experimental data fit well to this model as illustrated by Table 3. The values of β

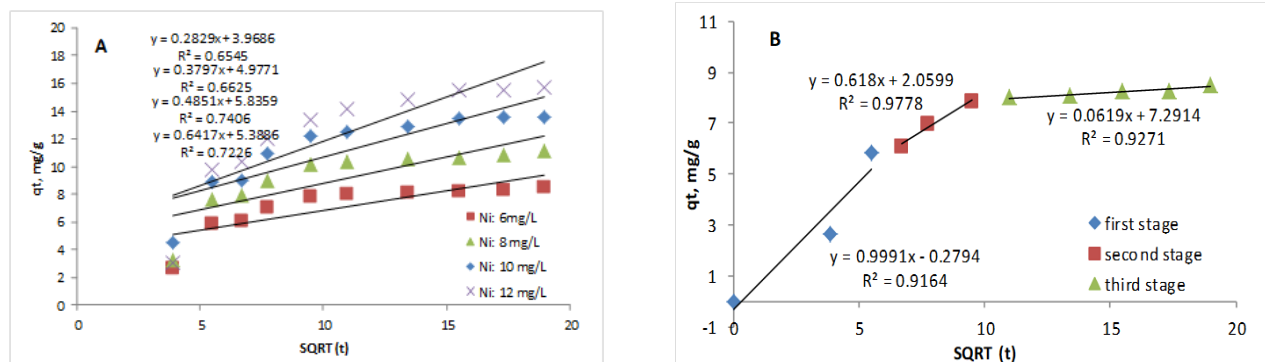


Fig. 6. Intraparticle diffusion for adsorption of nickel onto fuller's earth.

introduced in Table 3 indicate a low adsorption rate [40]. As observed in case of fitting the experimental data to the pseudo-second order model, there is no linear relationship between the initial concentration of adsorbate ions and the initial rate constant of the Elovich model (α) for both chromium and nickel ions. Another important feature of the Elovich model refers to the relation with the adsorbate ion diffusion. If the experimental data fits well to this model, then the diffusion is the rate limiting step of the adsorption process [41].

Adsorption mechanisms

The design of a successful adsorption system requires the prediction of the rate controlling mechanism. The adsorption of adsorbate molecules/ions in aqueous media takes place through four consecutive steps. First, the adsorbate species migrate through the bulk of the liquid to the stagnant film surrounding the adsorbent surface.

Fig. 6 presents the graphical fittings of the experimental data to the intraparticle diffusion model for nickel while Table 3 introduces the kinetic parameters calculated on the ground of this model. As seen from the figure the plots referring to the four tested concentrations are not linear within the whole time range. That may be explained by the presence of more than one process affecting the adsorption [42]. Fig. 6 (b) contains the lines obtained by fitting the data of nickel adsorption to the intraparticle diffusion model (an initial nickel concentration of 6 mg/L). The plots show that the adsorption involves three successive stages: external mass transference or boundary layer diffusion of adsorbate ions, a gradual adsorption stage where the intraparticle diffusion is rate determining, and the stage of reaching

a dynamic equilibrium where the intraparticle diffusion slows down due to the extremely low ion concentration in the aqueous phase [3, 43].

The low values of R^2 and the deviation from the origin in case of nickel ions adsorption data (for the four tested concentrations) suggest that the intraparticle diffusion controls the adsorption up to a certain degree, but it is not the rate controlling step. Generally, constant C indicates the thickness of the boundary layer - a higher C value corresponds to a thicker boundary layer. The value of C at an initial concentration of 12 mg/L is equal to 5.3886 mg/g and 0.0933 for nickel and chromium, respectively. This indicates that there is a greater boundary effect in case of nickel ions adsorption and hence a greater contribution of the surface sorption to the rate determining step [44]. It must be noted that the increase of the initial ion concentration results in an increase of both the rate constant and the thickness of the boundary layer.

Table 3 illustrates the fitting of experimental data to the Boyd's model for nickel ions adsorption. It is clear that the dependences are linear with high values of R^2 . That confirms the previously discussed results describing the intraparticle diffusion. Accordingly, the surface diffusion influences considerably the overall adsorption rate. It can be concluded that the fitting of the experimental data to the kinetic models reveals that both film diffusion and intraparticle diffusion control the adsorption of nickel ions on fuller's earth.

The fitting of the experimental data in case of chromium ions adsorption to the intraparticle diffusion model for the four tested concentrations shows a single regime of a linear behavior. This linearity is maintained throughout the adsorption period.

Moreover, the values of C are very near to zero indi-

Table 4. Comparison of the adsorption capacities of different adsorbents in respect to nickel and chromium ions adsorption.

Dye	Adsorbent	q_e , mg/g	Reference
<i>Nickel</i>	polymer	59.40	[48]
	Granular activated carbon	7.657	[49]
	Activated carbon	69.49	[50]
	Maghnite clay	18.95	[51]
	Saw dust	22.47	[52]
	Bael tree leaf	1.527	[53]
	fuller's earth	50	This work
<i>Chromium</i>	Modified activated carbon	71	[54]
	Clay	15.67	[55]
	Modified tea waste	75.76	[56]
	Shredded tyre	3.283	[57]
	Activated carbon	0.935	[58]
	L-Cysteine Magnetite Nanoparticles	34.48	[59]
	Longan seed	35.02	[60]
	fuller's earth	20	This work

cating that the effect of the boundary layer is minute and the intraparticle diffusion is the main controlling factor of the adsorption [45]. Regarding the effect of the initial chromium ion concentration on the rate constant for the intraparticle diffusion model (K_{id}), it is seen that there is a linear relationship between these two parameters (a data is not shown). The highest rate is obtained at the highest initial concentration due to the high driving force.

Table 3 indicates that the experimental data fit well to the Boyd model. This may indicate that the external mass transfer resistance (film-diffusion) has a certain effect on the adsorption or is only significant for a very short time period at the beginning of the diffusion since the boundary layer is very thin. The latter fact is illustrated by the intraparticle diffusion model [46].

Comparison of the fuller's earth adsorption capacity with that of other adsorbents

Researchers use different experimental conditions (e.g. pH, an adsorbent dose, a temperature, an initial adsorbate concentration, a stirring speed, a design of the adsorption reactor, etc.) and different physic-chemical properties of the adsorbents (i.e. porosity, density, a particle size, a surface area, a pore size and volume, moisture content, etc.) to conduct their adsorption tests. Accordingly, different adsorption capacities of a single adsorbent can be found in the literature. That is why it is difficult to compare the adsorption parameters of a given

adsorbate [47]. However, some comparisons still can be made. Table 4 depicts the comparison of the adsorption capacity of the current adsorbent (fuller's earth) with that of other adsorbents reported in the literature. It can be concluded that the fuller's earth has an adsorption capacity comparable to that of many other adsorbents.

CONCLUSIONS

The adsorption of chromium and nickel ions on fuller's earth is found to be of a chemical nature. The experimental data fit well to the pseudo second order and the Elovich models. It can be concluded that the chromium ions adsorption is predominantly controlled by intraparticle diffusion, while external and internal diffusion control the adsorption of nickel ions. The adsorption capacity in respect to both adsorbates is high suggesting that the fuller's earth is a potential adsorbent for similar heavy metals.

REFERENCES

1. R. Labied, O. Benturki, A.Y. Eddine Hamitouche, A. Donnot, Adsorption of hexavalent chromium by activated carbon obtained from a waste lignocellulosic material (*Ziziphus jujuba* cores): Kinetic, equilibrium, and thermodynamic study, *Adsorpt. Sci. Technol.*, 36, 2018, 1066-1099. doi:10.1177/0263617417750739.

2. T. Chen, Z. Zhou, S. Xu, H. Wang, W. Lu, Adsorption behavior comparison of trivalent and hexavalent chromium on biochar derived from municipal sludge, *Bioresour. Technol.*, 190, 2015, 388-394. doi:10.1016/j.biortech.2015.04.115.
3. J.R. de Andrade, M.G.C. da Silva, M.L. Gimenes, M.G.A. Vieira, Bioadsorption of trivalent and hexavalent chromium from aqueous solutions by sericin-alginate particles produced from *Bombyx mori* cocoons, *Environ. Sci. Pollut. Res.*, 2018, 1-16. doi:10.1007/s11356-018-2651-5.
4. Z. Wen, Y. Zhang, S. Guo, R. Chen, Facile template-free fabrication of iron manganese bimetal oxides nanospheres with excellent capability for heavy metals removal, *J. Colloid Interface Sci.*, 486, 2017, 211-218. doi:10.1016/j.jcis.2016.09.026.
5. J. Cancelo-González, D. Martiñá-Prieto, D. Hernández-Huerta, M.T. Barral, Metal removal by pine bark compost using a permeable reactive barrier device at laboratory scale, *Environ. Chem.*, 14, 2017, 310-318. doi:10.1071/EN17028.
6. N. Singh, K. Gupta, Adsorption of Heavy Metals: A Review, *Int. J. Innov. Res. Sci., Eng. Technol.*, 5, 2016, 2267-2281. doi:10.15680/IJIR-SET.2016.050146.
7. J. Cui, Y. Li, J. Meng, C. Zhong, P. Wang, Synthesis of chelating polyamine fibers and their adsorption properties for nickel(II) ions from aqueous solution, *RSC Adv.*, 7, 2017, 40392-40400. doi:10.1039/C7RA06935A.
8. P.M. Kopittke, C.J. Asher, F.P.C. Blamey, N.W. Menzies, Tolerance of two perennial grasses to toxic levels of Ni²⁺, *Environ. Chem.*, 5, 2008, 426-434. doi:10.1071/EN08054.
9. Y. Gopalapillai, C.L. Chakrabarti, D.R.S. Lean, Assessing toxicity of mining effluents: Equilibrium- and kinetics-based metal speciation and algal bioassay, *Environ. Chem.*, 5, 2008, 307-315. doi:10.1071/EN08027.
10. R. Kumar, M.O. Ansari, A. Alshahrie, R. Darwesh, N. Parveen, S.K. Yadav, M.A. Barakat, M.H. Cho, Adsorption modeling and mechanistic insight of hazardous chromium on para toluene sulfonic acid immobilized-polyaniline@CNTs nanocomposites, *J. Saudi Chem. Soc.*, 2018, doi:10.1016/j.jscs.2018.06.005.
11. P.A. Kobielska, A.J. Howarth, O.K. Farha, S. Nayak, Metal-organic frameworks for heavy metal removal from water, *Coord. Chem. Rev.*, 358, 2018, 92-107. doi:10.1016/j.ccr.2017.12.010.
12. T.E. Khalil, H. Altaher, R. Abubeah, Adsorptive removal of Cu (II) ions by date pits: Kinetic and equilibrium studies, *Environ. Eng. Manag. J.*, 15, 2016, 2719-2732.
13. H. Altaher, F. Al-Oufi, Y. Magdy, M. Hassan, Microwave against thermal treatment for manufacturing of activated carbon from agricultural wastes and its use to adsorb methylene blue - equilibrium and kinetic studies, *Yanbu J. Eng. Sci.*, 11, 2015, 29-42.
14. Y.M. Magdy, H. Altaher, E. ElQada, Removal of three nitrophenols from aqueous solutions by adsorption onto char ash: equilibrium and kinetic modeling, *Appl. Water Sci.*, 8, 2018, 26, doi:10.1007/s13201-018-0666-1.
15. Y.H. Magdy, H. Altaher, Kinetic analysis of the adsorption of dyes from high strength wastewater on cement kiln dust, *J. Environ. Chem. Eng.*, 6, 2018, 834-841, doi:10.1016/j.jece.2018.01.009.
16. Y.H. Magdy, H. Altaher, E.A. Abdelghany, Equilibrium and kinetic modeling for the adsorption of three phenolic compounds onto cement kiln dust, *J. Mater. Environ. Sci.*, 9, 2018, doi:10.26872/jmes.2018.9.2.63.
17. H. Altaher, T.E. Khalil, R. Abubeah, The effect of dye chemical structure on adsorption on activated carbon: A comparative study, *Color. Technol.*, 130, 2014, 205-214. doi:10.1111/cote.12086.
18. E.E. Ebrahiem, H. Altaher, E.A. Abdelghany, Y.H. Magdy, Packed Bed Column for Adsorption of Aqueous Phenols on Cement Kiln Dust, *J. Hazardous, Toxic, Radioact. Waste.*, 22, 2018, 04018009. doi:10.1061/(ASCE)HZ.2153-5515.0000401.
19. C. Parsons, Fuller's Earth, first, Government Printing Office, Bureau of Mines, Washington, 1913.
20. R. Abubeah, H. Altaher, T.E. Khalil, Removal of hexavalent chromium using two innovative adsorbents, *Environ. Eng. Manag. J.*, 17, 2018, 1621-1634.
21. Y.S. Ho, G. McKay, Kinetic Models for the Sorption of Dye from Aqueous Solution by Wood, *Process Saf. Environ. Prot.*, 76, 1998, 183-191. doi:10.1205/095758298529326.
22. Y. Yamamoto, N. Fujiwara, N. Asao, $Z \sim H / C = C = Ch =$, *J. Sanit. Eng. Div.*, 36, 1995, 2811-2814. doi:10.1080/002689796173345.

23. A.E. Ofomaja, Intraparticle diffusion process for lead(II) biosorption onto mansonia wood sawdust, *Bioresour. Technol.*, 101, 2010, 5868-5876. doi:10.1016/j.biortech.2010.03.033.
24. D.S. Rekunge, K.S. Indalkar, G.U. Chaturbhuj, Activated Fuller's earth as an inexpensive, eco-friendly, efficient catalyst for the synthesis of 5-aryl 1-H-tetrazole via [3+2] cycloaddition of nitriles and sodium azide, *Tetrahedron Lett.*, 57, 2016, 5815-5819. doi:10.1016/j.tetlet.2016.11.049.
25. G. Atun, G. Hisarli, W.S. Sheldrick, M. Muhler, Adsorptive removal of methylene blue from colored effluents on fuller's earth, *J. Colloid Interface Sci.*, 261, 2003, 32-39. doi:10.1016/S0021-9797(03)00059-6.
26. P. Thakur, R.K. Garg, New developing reagent for latent fingerprint visualization: Fuller's earth (Murtani Mitti), *Egypt. J. Forensic Sci.*, 6, 2016, 449-458. doi:10.1016/j.ejfs.2016.11.007.
27. J. Shah, M. Rasul Jan, M. Zeeshan, M. Imran, Kinetic, equilibrium and thermodynamic studies for sorption of 2,4-dichlorophenol onto surfactant modified fuller's earth, *Appl. Clay Sci.*, 143, 2017, 227-233. doi:10.1016/j.clay.2017.03.040.
28. A.K. Bajpai, N. Vishwakarma, Adsorption of polyvinylalcohol onto Fuller's earth surfaces, *Colloids Surfaces A Physicochem. Eng. Asp.*, 220, 2003, 117-130. doi:10.1016/S0927-7757(03)00073-6.
29. O.D. Beltran-Pérez, A. Hormaza-Anaguano, B. Zuluaga-Diaz, S.A. Cardona-Gallo, Structural modification of regenerated fuller earth and its application in the adsorption of anionic and cationic dyes adsorción de colorantes catiónicos y aniónicos, *Dyna*, 82, 2015, 165-171. doi:http://dx.doi.org/10.15446/dyna.v82n189.42954.
30. V. Díaz-Blancas, R. Ocampo-Pérez, R. Leyva-Ramos, P.A. Alonso-Dávila, A.I. Moral-Rodríguez, 3D modeling of the overall adsorption rate of metronidazole on granular activated carbon at low and high concentrations in aqueous solution, *Chem. Eng. J.*, 349, 2018, 82-91. doi:10.1016/j.cej.2018.05.076.
31. R. Yadav, A.K. Sharma, J.N. Babu, Sorptive removal of arsenite [As(III)] and arsenate [As(V)] by fuller's earth immobilized nanoscale zero-valent iron nanoparticles (F-nZVI): Effect of Fe0 loading on adsorption activity, *J. Environ. Chem. Eng.*, 4, 2016, 681-694. doi:10.1016/j.jece.2015.12.019.
32. A.E. Ofomaja, Kinetic study and sorption mechanism of methylene blue and methyl violet onto mansonia (*Mansonia altissima*) wood sawdust, *Chem. Eng. J.*, 143, 2008, 85-95. doi:10.1016/j.cej.2007.12.019.
33. Y.S. Ho, G. McKay, Pseudo-second order model for sorption processes, *Process Biochem.*, 34, 1999, 451-465. doi:10.1016/S0032-9592(98)00112-5.
34. L. Bulgariu, D. Bulgariu, Functionalized soy waste biomass - A novel environmental-friendly biosorbent for the removal of heavy metals from aqueous solution, *J. Clean. Prod.*, 197, 2018, 875-885, doi:10.1016/j.jclepro.2018.06.261.
35. M.F. Cheira, B.M. Atia, M.N. Kouraim, Uranium(VI) recovery from acidic leach liquor by Ambersep 920U SO 4 resin: Kinetic, equilibrium and thermodynamic studies, *J. Radiat. Res. Appl. Sci.*, 10, 2017, 307-319. doi:10.1016/j.jrras.2017.07.005.
36. Woodard & Curran Inc., *Industrial Waste Treatment Handbook*, 2006. doi:10.1016/B978-075067963-3/50011-4.
37. K.G. Quiton, B. Doma, C.M. Futralan, M.W. Wan, Removal of chromium(VI) and zinc(II) from aqueous solution using kaolin-supported bacterial biofilms of Gram-negative *E. coli* and Gram-positive *Staphylococcus epidermidis*, *Sustain. Environ. Res.*, 28, 2018, 206-213. doi:10.1016/j.serj.2018.04.002.
38. F.V.A. Dutra, B.C. Pires, T.A. Nascimento, K.B. Borges, Functional polyaniline/multiwalled carbon nanotube composite as an efficient adsorbent material for removing pharmaceuticals from aqueous media, *J. Environ. Manag.* 221, 2018, 28-37. doi:10.1016/j.jenvman.2018.05.051.
39. F.C. Wu, R.L. Tseng, R.S. Juang, Characteristics of Elovich equation used for the analysis of adsorption kinetics in dye-chitosan systems, *Chem. Eng. J.*, 150, 2009, 366-373, doi:10.1016/j.cej.2009.01.014.
40. Z. Ding, Q. Wang, X. Hu, Extraction of Heavy Metals from Water-Stable Soil Aggregates Using EDTA, *Procedia Environ. Sci.*, 18, 2013, 679-685, doi:10.1016/j.proenv.2013.04.092.
41. C. Chakrapani, C.S. Babu, K.N.K. Vani, K.S. Rao, Adsorption Kinetics for the Removal of Fluoride from Aqueous Solution by Activated Carbon Adsorbents Derived from the Peels of Selected Citrus Fruits, *E-Journal Chem.*, 7, 2010, S419-S427, doi:10.1155/2010/582150.
42. W.H. Cheung, Y.S. Szeto, G. McKay, Intraparticle diffusion processes during acid dye adsorption onto

- chitosan, *Bioresour. Technol.*, 98, 2007, 2897-2904, doi:10.1016/j.biortech.2006.09.045.
43. R. Baccar, P. Blázquez, J. Bouzid, M. Feki, M. Sarrà, Equilibrium, thermodynamic and kinetic studies on adsorption of commercial dye by activated carbon derived from olive-waste cakes, *Chem. Eng. J.*, 165, 2010, 457-464, doi:10.1016/j.cej.2010.09.033.
44. A. Adewuyi, F.V. Pereira, Nitrilotriacetic acid functionalized *Adansonia digitata* biosorbent: Preparation, characterization and sorption of Pb (II) and Cu (II) pollutants from aqueous solution, *J. Adv. Res.*, 7, 2016, 947-959, doi:10.1016/j.jare.2016.10.001.
45. M. Schwaab, E. Steffani, E. Barbosa-Coutinho, J.B. Severo Júnior, Critical analysis of adsorption/diffusion modelling as a function of time square root, *Chem. Eng. Sci.*, 173, 2017, 179-186, doi:10.1016/j.ces.2017.07.037.
46. R. Neubauer, M. Husmann, C. Weinlaender, N. Kienzl, E. Leitner, C. Hochenauer, Acid base interaction and its influence on the adsorption kinetics and selectivity order of aromatic sulfur heterocycles adsorbing on Ag-Al₂O₃, *Chem. Eng. J.*, 309, 2017, 840-849, doi:10.1016/j.cej.2016.10.094.
47. R.B. Garcia-Reyes, J.R. Rangel-Mendez, Adsorption kinetics of chromium(III) ions on agro-waste materials, *Bioresour. Technol.*, 101, 2010, 8099-8108, doi:10.1016/j.biortech.2010.06.020.
48. H. Ahmad Panahi, M. Samadi Zadeh, S. Tavangari, E. Moniri, J. Ghassemi, Nickel adsorption from environmental samples by ion imprinted aniline-formaldehyde polymer, *Iran. J. Chem. Chem. Eng.*, 31, 2012, 35-44.
49. D. Lakherwal, V.K. Rattan, H.P. Singh, Studies on Adsorption of Nickel by Activated Carbon in a Liquid Fluidised Bed Reactor, *Can. Chem. Trans.*, 4, 2016, 121-132, doi:10.13179/canchemtrans.2016.04.01.0264.
50. R.M. Shrestha, M. Varga, I. Varga, A.P. Yadav, B.P. Pokharela, R.R. Pradhananga, Removal of Ni (II) from Aqueous Solution by Adsorption onto Activated Carbon Prepared from Lapsi (*Choerospondias axillaris*) Seed Stone Preparation of Adsorbents, *J. Inst. Eng.*, 9, 2014, 166-174.
51. M.A. Zenasni, S. Benfarhi, A. Merlin, S. Molina, B. George, B. Meroufel, Adsorption of nickel in aqueous solution onto natural maghnite, *Mater. Sci. Appl.*, 4, 2013, 153-161, doi:10.4236/msa.2013.42018.
52. M.R. Samarghandi, S. Azizian, M.S. Siboni, S.J. Jafari, S. Rahimi, Removal of divalent nickel from aqueous solutions by adsorption onto modified holly sawdust: equilibrium and kinetics, *Iranian J. Environ. Health Sci. Eng.*, 8, 2011, 181-188.
53. P.S. Kumar, K. Kirthika, Equilibrium and kinetic study of adsorption of nickel from aqueous solution onto bael tree leaf powder, *J. Eng. Sci. Technol.*, 4, 2009, 351-363.
54. A.A. Attia, S.A. Khedr, S.A. Elkholy, Adsorption of chromium ion (VI) by acid activated carbon, *Brazilian J. Chem. Eng.*, 27, 2010, 183-193. doi:10.1590/S0104-66322010000100016.
55. A. Ksakas, A. Loqman, B. El Bali, M. Taleb, A. Kherbeche, The adsorption of Cr (VI) from aqueous solution by natural materials, *J. Mater. Environ. Sci.*, 6, 2015, 2003-2012.
56. S. Fan, Y. Wang, Y. Li, J. Tang, Z. Wang, J. Tang, X. Li, K. Hu, Facile synthesis of tea waste/Fe₃O₄ nanoparticle composite for hexavalent chromium removal from aqueous solution, *RSC Adv.*, 7, 2017, 75767590, doi:10.1039/C6RA27781K.
57. K.S.P. Kumar, E.C.N. Peter, Adsorption of chromium (VI) from aqueous solutions by different admixtures - A batch equilibrium test study, *J. Eng. Sci. Technol.*, 9, 2014, 410-422.
58. L. Shifera, K. Siraj, A. Yifru, Adsorption of lead (II) and chromium (VI) onto activated carbon prepared from pineapple peel: Kinetics and thermodynamic study, *Indian J. Chem. Technol.*, 24, 2017, 145-152.
59. Y. Bagbi, A. Sarswat, D. Mohan, A. Pandey, P.R. Solanki, Lead and Chromium Adsorption from Water using L-Cysteine Functionalized Magnetite (Fe₃O₄) Nanoparticles, *Sci. Rep.*, 7, 2017, doi:10.1038/s41598-017-03380-x.
60. J. Yang, M. Yu, W. Chen, Adsorption of hexavalent chromium from aqueous solution by activated carbon prepared from longan seed: Kinetics, equilibrium and thermodynamics, *J. Ind. Eng. Chem.*, 21, 2015, 414-422, doi:10.1016/j.jiec.2014.02.054.